Generalized Structural Description of Calcium–Sodium Aluminosilicate Hydrate Gels: The Cross-Linked Substituted Tobermorite Model

Generalized Structural Description of Calcium-Sodium Aluminosilicate Hydrate gels: The Crosslinked Substituted Tobermorite Model

Rupert J. Myers [1,2], Susan A. Bernal [1,2], Rackel San Nicolas [2], John L. Provis [1,2]*

[1] Department of Materials Science and Engineering, Sir Robert Hadfield Building, Mappin St, University of Sheffield, Sheffield S1 3JD, UK

[2] Department of Chemical & Biomolecular Engineering, University of Melbourne, Victoria 3010, Australia

* To whom correspondence should be addressed. Email jprovis@sheffield.ac.uk, phone +44 114 222 5490, fax +44 114 222 5943

Abstract

Structural models for the primary strength and durability-giving reaction product in modern cements, a calcium (alumino)silicate hydrate gel, have previously been based solely on non-crosslinked tobermorite structures. However, recent experimental studies of laboratory-synthesized and alkali-activated slag (AAS) binders have indicated that the calcium-sodium aluminosilicate hydrate (C-(N)-A-S-H) gel formed in these systems can be significantly crosslinked. Here, we propose a model that describes the C-(N)-A-S-H gel as a mixture of crosslinked and non-crosslinked tobermorite-based structures (the Crosslinked Substituted Tobermorite Model, CSTM), which can more appropriately describe the spectroscopic and density information available for this material. Analysis of the phase assemblage and Al coordination environments of AAS binders shows that it is not possible to fully account for the chemistry of AAS by use of the assumption that all of the tetrahedral Al is present in a tobermorite-type C-(N)-A-S-H gel, due to the structural constraints of the gel. Application of the CSTM can for the first time reconcile this information, indicating the presence of an additional activation product that contains highly connected four-coordinated silicate

and aluminate species. The CSTM therefore provides a more advanced description of the chemistry and structure of calcium-sodium aluminosilicate gel structures than that previously established in the literature.

Keywords: *Alkali activated slag; Cement hydration products; Calcium-sodium aluminosilicate hydrate; Tobermorite-like gels; Sublattice modeling*

1. Introduction

Historically, the most common binder gels used in the construction industry have been produced entirely from Portland cement (PC), which is a material that dates back nearly two hundred years.[1] The main hydration product in the binding phase in PC systems is a Ca-rich ($1.5 \leq Ca/Si \leq 2$) calcium silicate hydrate (C-S-H) gel,[2] which is thought to be comprised of non-crosslinked tobermorite and jennite-like structures.[3] However, it is common for modern cements to replace a large proportion of PC clinker with supplementary cementitious materials for environmental and performance (durability and strength) reasons,[4] which can greatly affect the chemistry of the binder gel because significant amounts of aluminum can be incorporated into the primary reaction product in these systems.[5]

One of the most common replacement materials in modern cements, ground granulated blast furnace slag (GBFS), can be activated by an alkaline solution, most commonly NaOH, KOH or $Na_2O{\cdot}mSiO_2{\cdot}xH_2O$, to form a hardened alkali-activated slag (AAS) binder.[6] This material has been developed and commercialized in many parts of the world as a high-performance alternative to PC with a reduced environmental footprint.[7] The major hydrate binding phase formed through the alkali activation of the GBFS precursor is an alkali charge-balanced aluminum substituted calcium silicate hydrate (C-(N)-A-S-H).[8,9] The C-(N)-A-S-H type gel is the main strength-giving phase in modern Portland cement blends admixed with high-aluminum containing materials [5] and in AAS.[7,10]

The solid phase assemblage of the binding phase in modern cements varies greatly with the supplementary cementitious material used,[5] but the nature of the C-(N)-A-S-H type gel formed in

these systems show a broad similarity not unlike the C-S-H product in PC binders.[11] Studies have typically limited the chemical composition to Ca-rich compositions within the CaO-SiO_2-Al_2O_3-H_2O(-Na_2O/K_2O) system [12,13] or to AAS systems, to understand the nature of the C-(N)-A-S-H gel [14] because the solid phase assemblage can vary significantly in modern cements. AAS is a particularly relevant model system because GBFS is a widely used replacement material in modern cements,[4] the binder gel in AAS sits within the Ca-rich composition region needed to form C-(N)-A-S-H,[5] and AAS chemistry is relatively well known.[7]

A detailed chemical-level understanding of AAS is a prerequisite for enabling the development and increased commercial uptake of AAS technology in modern civil infrastructure, but this information has not yet been fully elucidated. This is due largely to the low crystallinity and complex chemical environments of the C-(N)-A-S-H type gel, which varies according to: i) the activator type and concentration;[15,16] ii) the composition and reactivity of the GBFS precursor;[17,18] iii) the method of binder synthesis;[19,20] and iv) the curing conditions to which the material is subjected.[15] Secondary phases also co-exist with C-(N)-A-S-H in hardened AAS, meaning that an understanding of the assemblage of solid phases present in AAS is essential for quantification of the chemistry and molecular structure of the binder. These secondary phases include hydrotalcite,[14,17] "aluminoferrite-mono" (AFm) type phases including strätlingite and C_4AH_{13},[14,18,21] the 'third aluminate hydrate' (TAH),[22] members of the hydrogarnet series including katoite,[15,21,23,24] and zeolites such as gismondine and heulandite.[12,23] These difficulties have necessitated the use of idealized models to represent the structure and chemistry of C-(N)-A-S-H gels in the past.

The C-(N)-A-S-H type gel in AAS has a relatively low calcium content compared to the C-S-H gels formed in PC ($Ca/(Si+Al) < 1.5$), and is generally described as being similar in structure to the calcium silicate hydrate phase C-S-H(I),[2,7] a poorly ordered form of 14Å tobermorite.[25] These materials contain 'dreierketten' units, which are repeating chain units of three silicate tetrahedra (Figure 1). The tobermorite mineral group contains various structures differentiated by their basal spacing

(14Å, 11Å or 9Å),[26] and 11Å tobermorites contain Si-O-Si cross-links between adjacent silicate chains while 14Å and 9Å tobermorites do not.[25,27] Hydrated 14Å tobermorite, also known as plombierite, has a bound water to Si ratio (H_2O/Si) of 7/6 and 0.5 atoms of interlayer calcium per dreierketten unit, giving an overall formula of $Ca_5Si_6O_{16}(OH)_2 \cdot 7H_2O$,[25] although small variations in chemical composition can exist.[2] There are two types of 11Å tobermorite; those that shrink during dehydration and contain interlayer calcium ions are termed 'normal', and those that do not shrink during dehydration and contain no interlayer calcium are called 'anomalous'.[27] The bound water content also varies, with a reduction in bound water content associated with a decrease in the interlayer spacing.[28] Merlino et al. [27] elucidated the structures of normal and anomalous 11Å tobermorites, and found that anomalous 11Å tobermorite has H_2O/Si = 5/6 and no interlayer calcium ($Ca_4Si_6O_{15}(OH)_2 \cdot 5H_2O$), whereas normal 11Å tobermorite also has H_2O/Si = 5/6 but an interlayer calcium content of 0.25 atoms per dreierketten unit ($Ca_{4.5}Si_6O_{16}(OH) \cdot 5H_2O$). In an earlier study, Merlino et al. [29] also analyzed 9Å tobermorite (riversideite), finding no bound water and an interlayer calcium content of 0.5 atoms per dreierketten, corresponding to a crystal chemical formula of $Ca_5Si_6O_{16}(OH)_2$.[29]

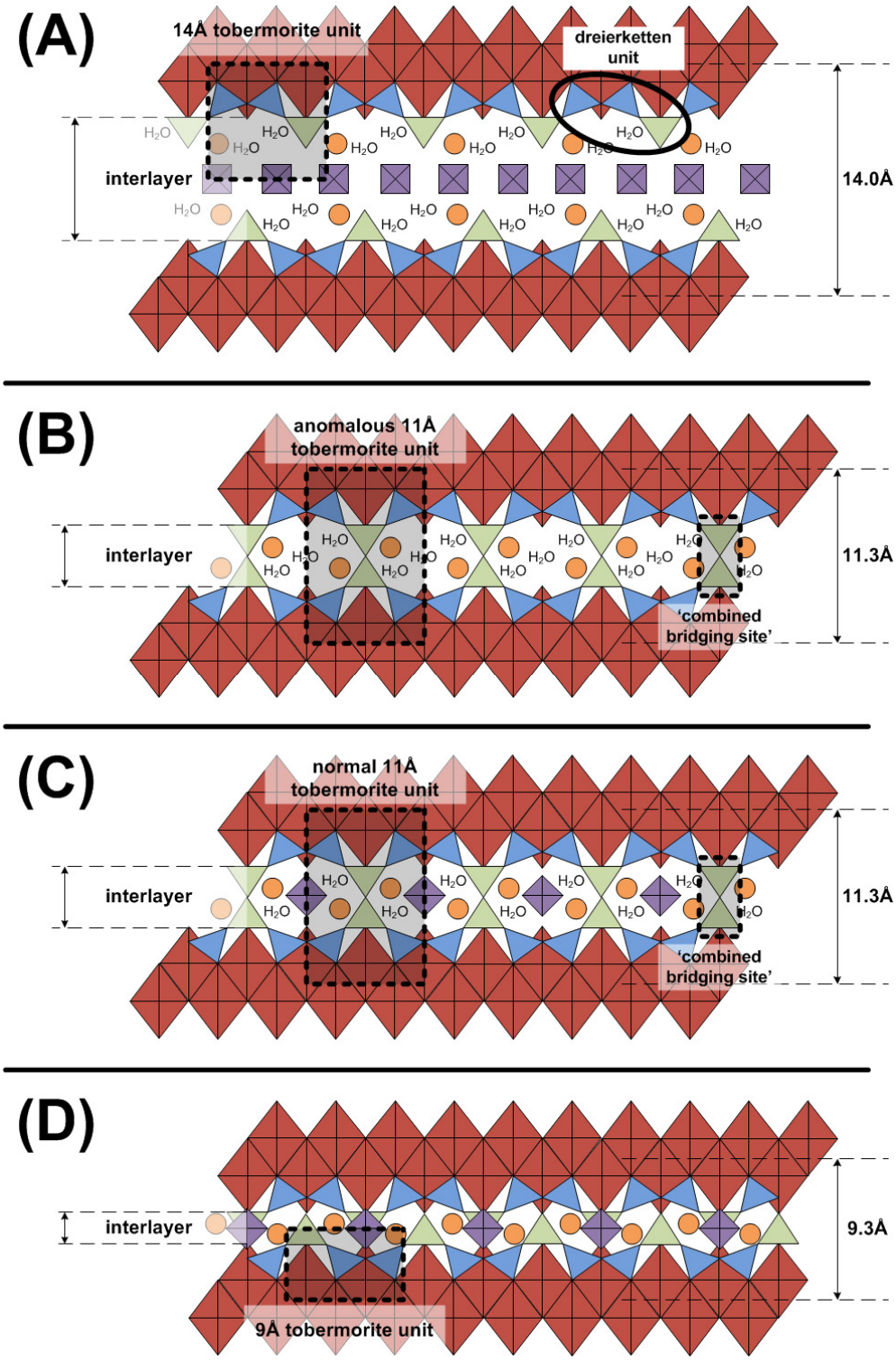

Figure 1. Schematic sublattice representations of A) 14Å tobermorite; B) anomalous 11Å tobermorite; C) normal 11Å tobermorite; D) 9Å tobermorite, all with 'infinite' chain length (no Si site vacancies). Paired and bridging tetrahedra are represented by blue and green triangles respectively, and intra-layer calcium, charge-balancing alkali cations and interlayer protons and/or calcium cations by the red oblongs, orange circles, and purple squares respectively. The specific size, location and number of these species are approximate; readers are referred to [25,27-29] for crystallographic structures. The combined bridging site is illustrated here to clarify its use in crosslinked tobermorite sublattice formulae. A dreierketten unit (three kinked repeating tetrahedra) is marked in A), and the interlayer spacing is also marked.

A simplified representation of these tobermorites, shown in terms of sublattice sites, is provided in Figure 1; the reader is referred to the contributions of Bonaccorsi et al. and Merlino et al.[25,27-29] for more comprehensive descriptions. Representation of these structures in terms of 'sublattice sites' is clearer from a modeling perspective, and has been used to construct structurally relevant formulae for these tobermorite phases, which are used to model the C-(N)-A-S-H type gel in this work.

The mean chain length (MCL) and Ca/Si ratio are known to have a significant effect on the mechanical properties of 14Å tobermorite,[30] and Oh et al. [31] found that while the model structure of 14Å tobermorite could replicate the mechanical properties of C-S-H(I) in the *a-b* plane (parallel to the Ca-O sheets), the response to compression in the *c* direction (perpendicular to the Ca-O sheet) was significantly different. This led to the suggestion that the molecular species present in the interlayer spacing between the silicate chains of 14Å tobermorite and C-S-H(I) differ, and that more work is needed to fully understand the interlayer region. A structural model that can describe the C-(N)-A-S-H type gel using a flexible definition of the MCL, Ca/Si ratio and interlayer spacing would enable a greater understanding of the mechanical behavior of the cements of the 21st century.

The purpose of this paper is therefore to develop rigorous analytical methods for the calculation of the composition and MCL of more aluminum-rich binders which are not well-described by the existing models based on the 14Å tobermorite structure.

2. Structural models for C-(N)-A-S-H

2.1. The current state of the art

The key value of a structural model is that the chemical composition and the MCL of the C-(N)-A-S-H product can be directly calculated from experimental data such as ^{29}Si magic angle spinning nuclear magnetic resonance (MAS NMR) spectral deconvolutions, and that the conceptual model can be validated by relating its predictions to independent experimental results. The 'Substituted General

Model' (SGM) of Richardson and Groves is widely used in cement chemistry,[32] describing a mixture of 14Å tobermorite, jennite and $Ca(OH)_2$ structures, and is shown in eq.(1):

$$Ca_X H_{(6n-2X)} \left(Si_{(1-a_0)} R_{a_0}\right)_{(3n-1)} O_{(9n-2)} \cdot I^{c+}_{\frac{a_0}{c}(3n-1)} \cdot zCa\left(OH\right)_2 \cdot mH_2O \quad (1)$$

Here, R is a trivalent cation in tetrahedral coordination (usually Al^{3+} or Fe^{3+}), I is a charge-balancing interlayer cation (such as Ca^{2+} or an alkali metal) with a positive charge of c, m defines the amount of bound interlayer water, n is the number of dreierketten units per 14Å tobermorite chain, and a_0 is the extent of substitution of I into the structure. The parameters X, z, a_0 and n are defined in terms of w (the degree of protonation of the chain units) and y (the content of $Ca(OH)_2$ in the C-(N)-A-S-H solid solution), according to eq.(2):[32]

$$\left.\begin{array}{c} X = 0.5\left(6n - w\right) \\ z = 0.5\left[w + n\left(y - 2\right)\right] \\ 0 \le a_0 \le \dfrac{n-1}{\left(3n-1\right)} \end{array}\right\} \quad (2)$$

Eq.(1) can then be rewritten in terms of sublattice sites, which is useful for thermodynamic modeling purposes.[33] This is achieved by limiting substitution to bridging sites, and selection of aluminum as the tetrahedrally coordinated trivalent cation (R) and sodium as the charge-balancing interlayer cation (I):

$$\left[\left(Ca\left(OH\right)_2\right)_{\left(\frac{u+y-2}{4}\right)}\right]_2 \cdot \left[\left(CaSiO_{3.5}\right)_2^-\right] \cdot \left[\left(Si_{(1-a)}Al_aO_2\right)_{(1-\nu)} \cdot \left(Na^+_{a(1-\nu)}\right) \cdot \left(Ca_{\left(1-\frac{u}{2}\right)}H_u\right)^{2+}\right] \cdot mH_2O \quad (3)$$

where a is the extent of substitution in bridging sites; $\nu = \dfrac{1}{n}$ ($0 \le \nu \le 1$), the ratio of chains to dreierketten units (a measure of chain site vacancies); and $u = \dfrac{w}{n}$, the amount of hydroxyl water (or equivalently the number of protons) per dreierketten unit. The MCL and Al/Si ratio can then be

calculated, using the assumption that the gel nanostructure resembles the structure of 14Å tobermorite, and the Ca/Si ratio can be determined from eq.(3), leading to eqs.(4-6):[14]

$$MCL_{[NC]} = \frac{2\left[Q^1 + Q^2 + \left(\frac{3}{2}\right)Q^2(1Al)\right]}{Q^1} \quad (4)$$

$$\left(Al/Si\right)_{[NC]} = \frac{\left(\frac{1}{2}\right)Q^2(1Al)}{Q^1 + Q^2 + Q^2(1Al)} \quad (5)$$

$$\left(Ca/Si\right)_{[NC]} = \frac{4+y}{4+2(1-v)(1-a)} \quad (6)$$

where [NC] denotes non-crosslinked C-(N)-A-S-H structures. In this work, the MCL is defined as the number of aluminosilicate tetrahedra per tobermorite chain. This model has replicated experimental (electron microscopic) observations of the chemical composition of the main hydrate phase in hydroxide-activated AAS paste.[19,34] There exist several other models based on tobermorite, jennite and $Ca(OH)_2$ type structures that can describe C-S-H type gels (and an excellent summary of these was given by Richardson [3]), but none are as flexible as the SGM for describing substitution within C-(N)-A-S-H gels.[3,11]

2.2. The need for an alternative structural representation of the C-(N)-A-S-H phase

While the SGM has generally been able to give a good description of the local structure and chemical composition of C-(N)-A-S-H gels,[11,19,34] recent experimental results have identified characteristics of AAS that support the formation of an alternative gel structure over the same range of chemical compositions.[8,16,35]

Thomas et al. [36] calculated the H_2O/Si ratio and density of a hypothetical calcium aluminum silicate hydrate (C-A-S-H) type gel with Ca/Si = 0.99 and Al/Si = 0.06 to be H_2O/Si = 0.97 ± 0.03, $\rho_{C\text{-}A\text{-}S\text{-}H}$ = 2.73 ± 0.02 g/cm^3 and V = 50.8 ± 0.6 cm^3/mol.[36] Those authors related their results to both 14Å and 11Å tobermorite structures, and found that the 11Å tobermorite representation predicted a molar volume 12% less than a C-A-S-H gel of similar composition, consistent with the significantly lower densities found in tobermorite structures than in C-S-H type gels. The opposite was found for the

14Å tobermorite; this model structure predicted a molar volume that was 4% greater than a C-S-H of similar composition. The calculated H_2O/Si value of the C-A-S-H was also more consistent with the lower H_2O/Si ratios found in 11Å tobermorites.[27] The proposed hypothetical chemical composition $(CaO)_{0.99}(Al_2O_3)_{0.06}(SiO_2)(H_2O)_{0.97}$ suggested by Thomas et al. can be represented either by 11Å tobermorite or a mixture of 14Å, 11Å and 9Å tobermorites.

Further support for the development of an alternative model describing the tobermorite structure of C-(N)-A-S-H type gels forming in AAS pastes can also be found in recent high resolution ^{29}Si MAS NMR results of silicate-activated slag systems, where the formation of cross-linked Si sites (Q^3 and Q^3(1Al)) is identified.[19,24,37,38] Q^3 type silica bonding environments can only be explained in tobermorite structural models by cross-linking between bridging sites in the silicate chains (as displayed in Figure 1). The small but non-zero concentration of Q^3 silicate species found in C-(N)-A-S-H [24,37] thus supports the description of the gel as a mixture of crosslinked (11Å tobermorite) and non-crosslinked (14Å and/or 9Å tobermorite) chains.

Thus, it is both appropriate and necessary to conceptualize and model the C-(N)-A-S-H phase in AAS in an alternative way, generalizing from the SGM of Richardson and Groves.[32] Here, we derive formulae representing 9Å, 11Å and 14Å tobermorite structures and the associated Ca/Si, Al/Si and MCL relationships, and validate the model by comparison with experimental data.

3. Derivation of a generalized model

3.1. Derivation of crosslinked tobermorite models

The derivation of an 11Å tobermorite model begins by defining a crosslinked tobermorite unit, as shown in Figure 1. The structural model described in this study excludes Al-O-Al bonding in bridging sites, considering the Al-avoidance principle of Loewenstein,[39,40] and leads to the same relationships for the Al/Si ratio and MCL for anomalous and normal 11Å tobermorites. This is expected because only the bound water and interlayer charge-balancing cation content differ between the normal and

anomalous forms of these minerals.[27] These relationships can be solved directly using spectral deconvolutions of ^{29}Si MAS NMR data, and are shown in eqs.(7-8):

$$MCL_{[C]} = \frac{4\left(Q^1 + Q^2 + Q^2\left(1Al\right) + Q^3 + 2Q^3\left(1Al\right)\right)}{Q^1} \tag{7}$$

$$\left(Al/Si\right)_{[C]} = \frac{Q^3(1Al)}{Q^1 + Q^2 + Q^2\left(1Al\right) + Q^3 + Q^3\left(1Al\right)} \tag{8}$$

where [C] denotes crosslinked C-(N)-A-S-H structures. An application of eqs.(7-8) to a crosslinked tobermorite species is provided in Appendix A.

A more detailed analysis is necessary to determine the calcium content and Ca/Si ratio of crosslinked tobermorite. By grouping the crosslinked bridging tetrahedra together to form a 'combined bridging site' (see Figure 1) and using sodium as the alkali charge-balancing species, the chemical formula of a crosslinked tobermorite unit can be expressed (equivalent to eq.(3) for the non-crosslinked case) according to eq.(9):

$$\left[\left(Ca\left(OH\right)_2\right)_{\left(\frac{u+y-2}{4}\right)}\right]_4 \cdot \left[\left(CaSiO_{3.5}\right)^-\right]_4 \cdot \left[\left(\left[SiO_{1.5}^+\right] \cdot \left[Si_{(1-\alpha)}Al_\alpha O_{1.5}^{(1-\alpha)+}\right] \cdot \left[Na_\alpha^{\alpha+}\right]\right)_{(1-\delta)} \cdot \left(Ca_\omega H_{2(1+\delta-\omega)}\right)^{2(1+\delta)+}\right]_1 \cdot mH_2O \tag{9}$$

where α is the fraction of aluminum substitution in crosslinked tobermorite, $\delta = \frac{1}{\sigma+1}$ is the fraction of combined bridging site vacancies per crosslinked tobermorite unit, σ is the number of crosslinked tobermorite units per chain, $\omega = 1 - \frac{u}{2}$ is the interlayer calcium content per crosslinked tobermorite unit, and all other parameters have the same definitions as in eqs.(1-3).

The extent of protonation is specified to maintain charge balance in eq.(9); the parameter describing the extent of protonation of (Al-substituted) silicate chains, u, has been replaced by a measure of the

concentration of calcium cations in the interlayer region, ω. This is consistent with the results of Merlino et al.,[29] who concluded that reductions in the basal spacing of crosslinked tobermorite species could be appropriately described by varying interlayer calcium contents. The introduction of ω into the model thus clarifies the importance of the interlayer calcium content in 11Å and 9Å tobermorites. It must also be noted that this substitution is possible because tobermorite solid-solutions contain no discrete $Ca(OH)_2$, i.e. $u + y = 2$,[11,32] thus u is not an independent parameter in eq.(9) for tobermorite-based structures.

The interlayer calcium content, and therefore the extent of protonation, is thus determined by the degree of aluminum substitution, the fraction of bridging site vacancies (or equivalently the chain length), and the type of crosslinked tobermorite structure. Eq.(9) can be rewritten using $u + y = 2$, leading to eq.(10) as a charge-balanced formula in terms of one dreierketten unit:

$$\left[\left(CaSiO_{3.5}\right)^{-}\right]_2 \cdot \left[\left(\left[SiO_{1.5}^{+}\right]\cdot\left[Si_{(1-\alpha)}Al_{\alpha}O_{1.5}^{(1-\alpha)+}\right]\cdot\left[Na_{\alpha}^{\alpha+}\right]\right)_{(1-\delta)} \cdot \left(Ca_{\omega}H_{2(1+\delta-\omega)}\right)^{2(1+\delta)+}\right]_{0.5} \cdot mH_2O \quad (10)$$

Giving:

$$\left(Ca/Si\right)_{[C]} = \frac{4+\omega}{4+\left(1-\delta\right)\left(2-\alpha\right)} \quad (11)$$

$$Ca/(Al+Si)_{[C]} = \frac{4+\omega}{2(3-\delta)} \quad (12)$$

$$0 \le \omega \le 1+\delta \quad (13)$$

Eq.(10) reduces to the chemical formula for non-substituted infinite chain length normal 11Å tobermorite, $Ca_{4.5}Si_6O_{16}(OH)\cdot 5H_2O$,[27] when ω, α, δ and H_2O/Si are 0.5, 0, 0, and 5/6 respectively. The formula for non-substituted infinite chain length anomalous 11Å tobermorite, $Ca_4Si_6O_{15}(OH)_2\cdot 5H_2O$,[27] is similarly obtained from eq.(10) when ω, α, δ and H_2O/Si are 0, 0, 0, and 5/6 respectively.

While non-substituted normal 11Å tobermorite was identified by Merlino et al. (2001) as containing 0.25 interlayer calcium atoms per dreierketten unit,[27] it is reasonable to suggest that the interlayer

calcium content will vary as a function of aluminum substitution. This has therefore been left variable in eq.(10). The parameters δ and α can then be determined from eqs.(14-15) using the relationships for the Al/Si ratio and MCL for crosslinked tobermorite species, as given in eqs.(7-8):

$$\delta = \frac{6}{MCL_{[C]} + 2} \tag{14}$$

$$\alpha = \frac{(Al/Si)_{[C]} \times \left[4+2(1-\delta)\right]}{\left[(Al/Si)_{[C]}+1\right] \times (1-\delta)} \tag{15}$$

3.2. Derivation of a non-crosslinked tobermorite model

A 9Å tobermorite consists of non-crosslinked silicate chains, and therefore can be represented according to the same basic formulation (eqs.(3-6)) used to describe the non-crosslinked 14Å tobermorite.[14] In this case eqs.(3,6) are rewritten in terms of φ, the interlayer calcium content per non-crosslinked tobermorite unit, setting $u + y = 2$ for consistency with the relationships derived for crosslinked tobermorites. The MCL and Al/Si relationships are the same for non-crosslinked 9Å and 14Å tobermorites. Eq.(3) can then be reformulated in terms of one dreierketten unit, leading to eqs.(16-18):

$$\left[\left(CaSiO_{3.5}\right)_2^-\right] \cdot \left[\left(\left[Si_{(1-a)}Al_aO_2\right] \cdot \left[Na_a^+\right]\right)_{(1-\nu)} \cdot \left(Ca_\varphi H_{2(1-\varphi)}\right)^{2+}\right] \cdot mH_2O \tag{16}$$

$$\left(Ca/Si\right)_{[NC]} = \frac{2+\varphi}{2+\left(1-\nu\right)\left(1-a\right)} \tag{17}$$

$$0 \le \varphi \le 1 \tag{18}$$

The Ca/(Si+Al) ratio is then:

$$Ca/(Si+Al)_{[NC]} = \frac{2+\varphi}{2+\left(1-\nu\right)} \tag{19}$$

Eq.(16) reduces to the chemical formula for non-substituted infinite chain length 9Å tobermorite, $Ca_5Si_6O_{16}(OH)_2$,[29] when φ, a, ν and H_2O/Si are 0.5, 0, 0, and 0 respectively. The formula for non-

substituted infinite chain length 14Å tobermorite, $Ca_5Si_6O_{16}(OH)_2 \cdot 7H_2O$,[25] is similarly recovered from eq.(16) when φ, a, v and H_2O/Si are 0.5, 0, 0, and 7/6 respectively.

The parameters v and a can be determined from eqs.(20-21) using the relationships for the Al/Si ratio and MCL of non-crosslinked tobermorite species, as given in eqs.(4-5):

$$v = \frac{3}{MCL_{[NC]} + 1} \tag{20}$$

$$a = \frac{\left[2+(1-v)\right] \times (Al/Si)_{[NC]}}{(1-v) \times \left[(Al/Si)_{[NC]} + 1\right]} \tag{21}$$

These formulae, eqs.(10-21), are suitable for modeling the C-(N)-A-S-H phase in the general case, and can be solved using structural parameters obtained from ^{29}Si MAS NMR spectral deconvolutions, as will be demonstrated in detail in section 4.

3.3. The 'Crosslinked Substituted Tobermorite Model'

It is reasonable to represent the C-(N)-A-S-H phase in AAS binders as a mixture of 14Å, 11Å and 9Å tobermorite structures,[8,19,36-38] as discussed in section 2.2. Here we propose a simple and flexible model, the 'Crosslinked Substituted Tobermorite Model' (CSTM), which can be used to determine the relative contributions of non-crosslinked and crosslinked tobermorites, and the chemical compositions and MCL of a particular C-(N)-A-S-H type gel. The CSTM only allows for aluminum substitution in bridging sites,[41] and does not include Al-O-Al bonding,[39] single tetrahedron vacancies in the combined bridging site, or incorporation of Q^0 or Q^1(1Al) species into the C-(N)-A-S-H phase.[41]

The fact that the CSTM does not allow single vacancies in the combined bridging site is worthy of further explanation. This is done to circumvent an explicit description of the two-coordinated bridging silicon (Q^2_B) sites that would arise if these species were allowed, and is possible because the C-(N)-A-S-H type gel is represented as a mixture of single chain and crosslinked structures. This is illustrated in Figure 2, which shows that a realistic section of crosslinked structure with a single

bridging site vacancy is conceptually equivalent to a mixture of non-crosslinked and crosslinked tobermorites in the CSTM formulation.

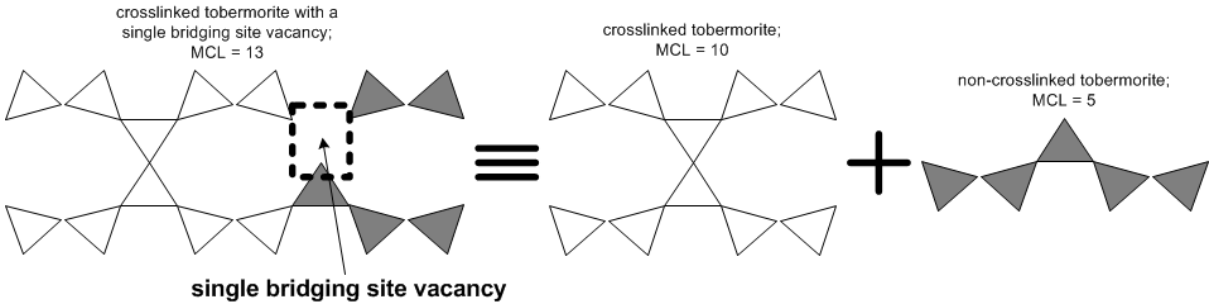

Figure 2. An illustration of how the CSTM represents single bridging site vacancies in AAS

The CSTM is derived using the following structural constraints: i) there are twice as many (Q^2+Q^2(1Al)) silicate species as there are (Q^3+Q^3(1Al)+$Al^{[4]}$) silicate species in crosslinked tobermorite; ii) the fraction of aluminum substitution into Q^3 type sites is equivalent to the ratio of Q^2(1Al) to Q^2 sites in crosslinked tobermorite, because aluminum is only substituted into bridging sites; and iii) the substitution of one $Al^{[4]}$ species into crosslinked tobermorite introduces one Q^3(1Al) and two Q^2(1Al) Si species. These assumptions and structural constraints are shown in Figure 3.

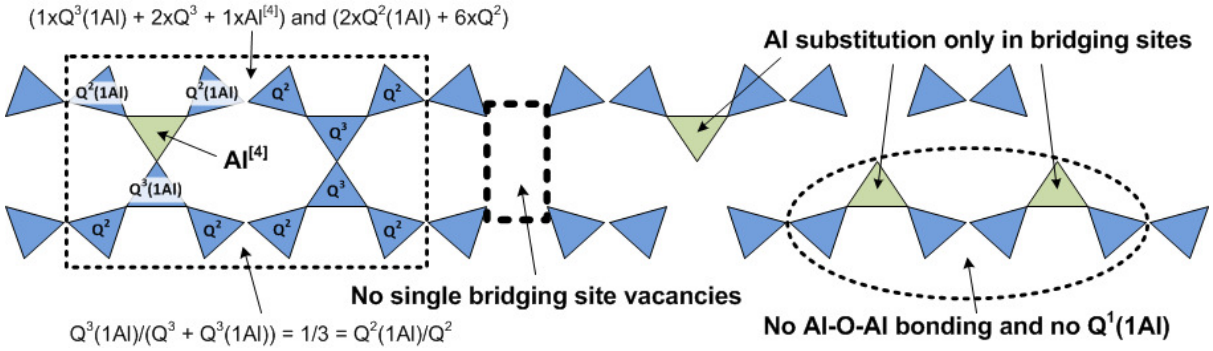

Figure 3. An illustration of the structural constraints and assumptions included in the CSTM

These structural constraints lead to eqs.(22-24):

$$2\left(Q^3_{[C]} + Q^3\left(1Al\right)_{[C]} + Al^{[4]}_{[C]}\right) = \left(Q^2_{[C]} + Q^2\left(1Al\right)_{[C]}\right) \quad (22)$$

$$\frac{Q^3\left(1Al\right)_{[C]}}{Q^3{}_{[C]} + Q^3\left(1Al\right)_{[C]}} = \frac{Q^2\left(1Al\right)_{[C]}}{Q^2_{[C]}} \quad (23)$$

$$Al^{[4]}_{[C]} = Q^3\left(1Al\right)_{[C]} \quad (24)$$

where $[C]$ denotes that the coordinated silicate species is present in crosslinked C-(N)-A-S-H. Eqs.(22-24) are solved to obtain eq.(25):

$$Q^2\left(1Al\right)_{[C]} = 2Q^3\left(1Al\right)_{[C]} \quad (25)$$

Eq.(25) is then used together with eqs.(26-29) to calculate the MCL and Al/Si molar ratios for non-crosslinked and crosslinked C-(N)-A-S-H products:

$$Q^3_{[C]} = Q^3_{total} \quad (26)$$

$$Q^3(1Al)_{[C]} = Q^3\left(1Al\right)_{total} \quad (27)$$

$$Q^1{}_{[C]} = \eta Q^1{}_{total} \quad (28)$$

$$Q^i_{[NC]} = Q^i_{total} - Q^i_{[C]} \quad (29)$$

where $[NC]$ denotes that the silicate species is present in non-crosslinked C-(N)-A-S-H species, η ($0 < \eta < 1$) is a parameter describing the partitioning of Q^1 species into non-crosslinked and crosslinked C-(N)-A-S-H type gel, adjusted to satisfy the structural constraints of the gel for the calculated Al-substitution extents (eqs.(15, 21)) and match experimentally observed chemical compositions (reported in section 4), and i ($0 \le i \le 4$) denotes the speciation environment of silica species in the C-(N)-A-S-H phase. The Al/Si and MCL values for non-crosslinked and crosslinked tobermorites can be calculated from eqs.(4-5) and eqs.(7-8) respectively, leading to eqs.(30-33), the relationships that describe the total amount of aluminum and silicon present, and average Al/Si and MCL values for the entirety of the C-(N)-A-S-H phase:

309 $$(Al+Si)_{[NC]} = Q^{1}{}_{[NC]} + \left(\tfrac{3}{2}\right) Q^{2}(1Al)_{[NC]} + Q^{2}{}_{[NC]} \quad (30)$$

310 $$(Al+Si)_{[C]} = Q^{1}{}_{[C]} + Q^{2}(1Al)_{[C]} + Q^{2}{}_{[C]} + 2Q^{3}(1Al)_{[C]} + Q^{3}{}_{[C]} \quad (31)$$

311 $$\left(Al/Si\right)_{C-(N)-A-S-H} = \frac{\left[\frac{\left(Al/Si\right)_{[NC]}}{\left(1+\left(Al/Si\right)_{[NC]}\right)}\right](Al+Si)_{[NC]} + \left[\frac{\left(Al/Si\right)_{[C]}}{\left(1+\left(Al/Si\right)_{[C]}\right)}\right](Al+Si)_{[C]}}{\left[\frac{1}{\left(1+\left(Al/Si\right)_{[NC]}\right)}\right](Al+Si)_{[NC]} + \left[\frac{1}{\left(1+\left(Al/Si\right)_{[C]}\right)}\right](Al+Si)_{[C]}} \quad (32)$$

312 $$MCL_{C-(N)-A-S-H} = \frac{MCL_{[NC]}MCL_{[C]}\left[(Al+Si)_{[NC]} + (Al+Si)_{[C]}\right]}{MCL_{[C]}(Al+Si)_{[NC]} + MCL_{[NC]}(Al+Si)_{[C]}} \quad (33)$$

313 Eqs.(32-33) are derived from the fractional concentrations of silicon and aluminum in 9Å, 11Å and
314 14Å tobermorite chains, i.e. $Al/Si = (1-Si)/Si$. The Ca/Si and Ca/(Al+Si) ratios are calculated
315 similarly, but vary depending on the level of interlayer calcium, the extent of protonation of the C-
316 (N)-A-S-H chains and the specific type of crosslinked C-(N)-A-S-H modeled:

317 $$\left(Ca/Si\right)_{C-(N)-A-S-H} = \frac{\left[\frac{\left(Ca/Si\right)_{[NC]}}{\left(1+\left(Al/Si\right)_{[NC]}\right)}\right](Al+Si)_{[NC]} + \left[\frac{\left(Ca/Si\right)_{[C]}}{\left(1+\left(Al/Si\right)_{[C]}\right)}\right](Al+Si)_{[C]}}{\left[\frac{1}{\left(1+\left(Al/Si\right)_{[NC]}\right)}\right](Al+Si)_{[NC]} + \left[\frac{1}{\left(1+\left(Al/Si\right)_{[C]}\right)}\right](Al+Si)_{[C]}} \quad (34)$$

318 $$Ca/(Al+Si)_{C-(N)-A-S-H} = \frac{\left[\frac{\left(Ca/Si\right)_{[NC]}}{\left(1+\left(Al/Si\right)_{[NC]}\right)}\right](Al+Si)_{[NC]} + \left[\frac{\left(Ca/Si\right)_{[C]}}{\left(1+\left(Al/Si\right)_{[C]}\right)}\right](Al+Si)_{[C]}}{(Al+Si)_{[NC]} + (Al+Si)_{[C]}} \quad (35)$$

319 where $\left(Ca/Si\right)_{[NC]}$ is given by eq.(17) and $\left(Ca/Si\right)_{[C]}$ can be calculated from eq.(11). Eqs.(34-35)
320 give the overall Ca/Si and Al/Si ratios for the assemblage of crosslinked and non-crosslinked
321 tobermorite species. The CSTM is also capable of accounting for the more general case where the
322 chemical compositions can be specified separately for 9Å, anomalous 11Å, normal 11Å and 14Å

tobermorites, but because the corresponding Ca/Si and Ca/(Al+Si) relationships are considerably more complicated than eqs.(34-35), these formulae are presented in Appendix B.

The following sections of the manuscript present the application of the CSTM to a series of sodium silicate-activated slag binders, as well as a discussion of the implications of the model results.

4. Application of the CSTM

A complete description of the experimental details for this investigation is given in Appendix C. The CSTM calculations are compared with experimental ^{27}Al and ^{29}Si MAS NMR and environmental scanning electron microscopy – energy dispersive X-ray spectroscopy (ESEM-EDS) results obtained for silicate-activated slag binders synthesized from a GBFS supplied by Zeobond Pty Ltd (Australia). The chemical composition and physical properties of the GBFS used are reported in Appendix C.

The ESEM-EDS results for the AAS pastes assessed are shown in Figures 4-5; ^{29}Si MAS NMR spectra are shown in Figure 6 and the results of the associated spectral deconvolutions are presented in Table 1. ^{27}Al MAS NMR spectra are shown in Figure 7 with corresponding spectral deconvolutions presented in Table 2. Discussion of the deconvolution procedures are given along with the experimental details in Appendix C.

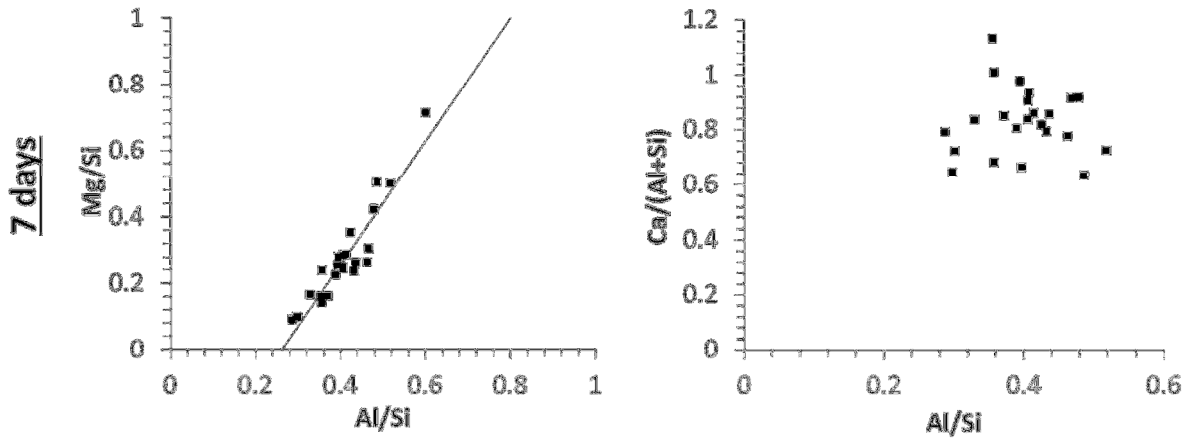

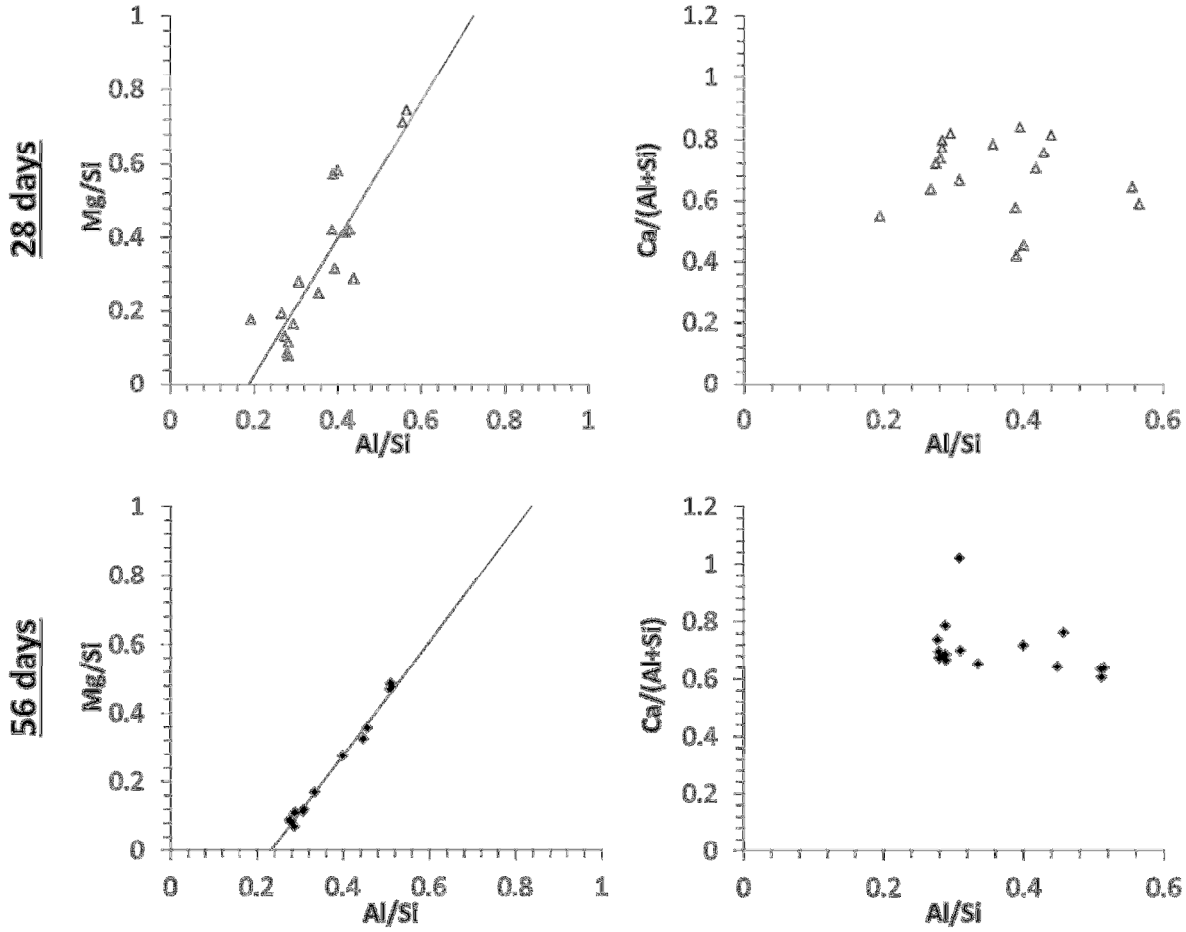

Figure 4. Molar ratios of alkali silicate-activated slag binder measured through ESEM-EDS, as a function of the time of curing

The binder composition data in Figure 5 show that the C-(N)-A-S-H phase is always present with at least one additional solid phase. Hydrotalcite has been identified through X-ray diffraction in silicate-activated slag pastes produced using similar raw materials to those used here,[24] consistent with Figures 4 and 5. However, the existence of additional calcium, aluminum and/or silicon-containing phases cannot be discounted purely on the basis of a good correlation between the observed chemistry of the AAS binder and a mixture of C-(N)-A-S-H type gel and hydrotalcite, as phases such as hydrogarnet and AFm are sometimes observable by X-ray diffraction in aged alkali-activated slag binders.[42]

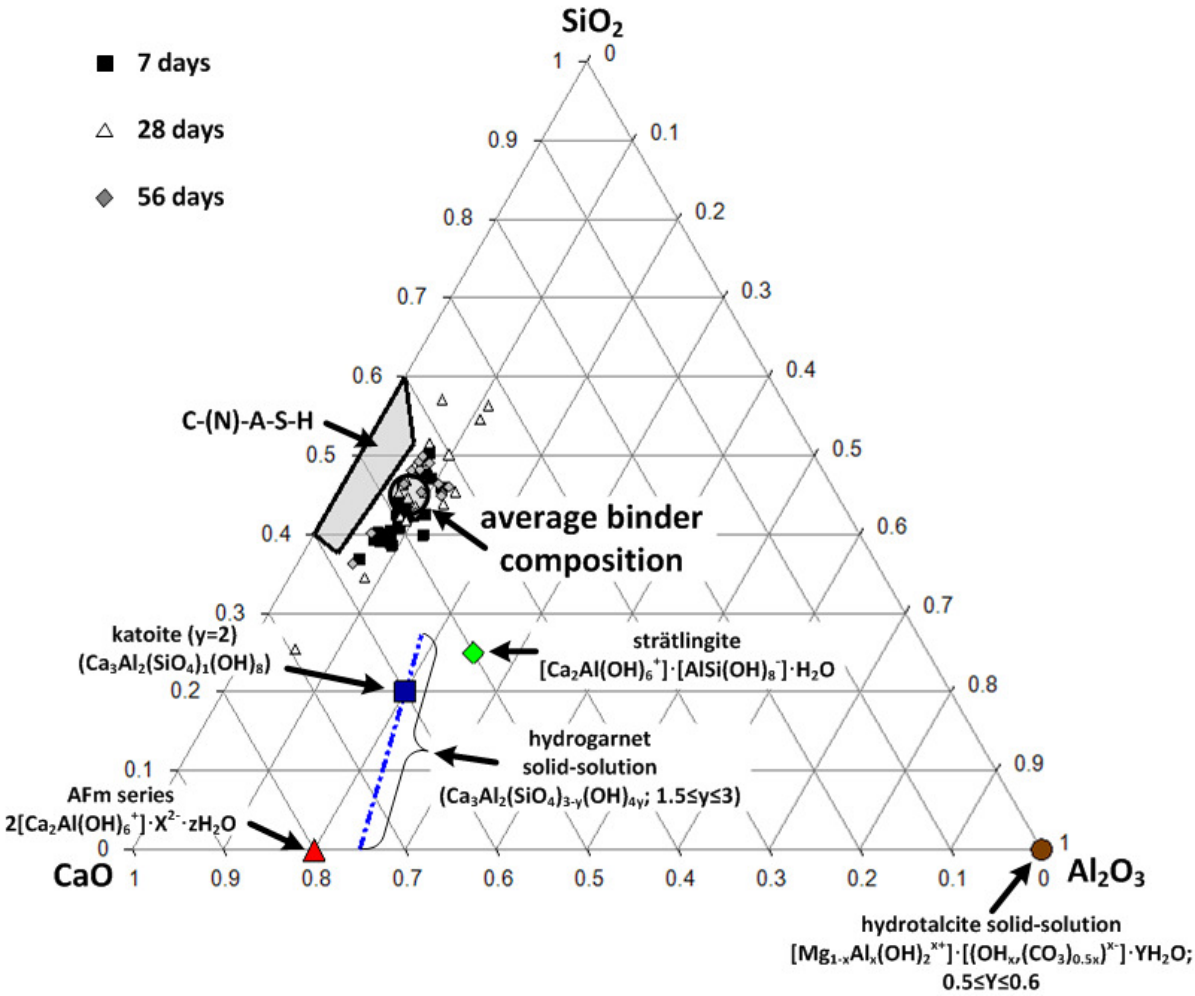

Figure 5. Projection of AAS chemistry onto the ternary CaO-SiO_2-Al_2O_3 system, showing elemental compositions of sodium silicate-activated slag binders measured by ESEM-EDS at different times of curing, along with the compositions of some model phases. The average composition of the binders is marked, assuming congruent dissolution of the reacted component of the slag, complete incorporation of the silica supplied by the activator into the binder, and without distinction between product phases

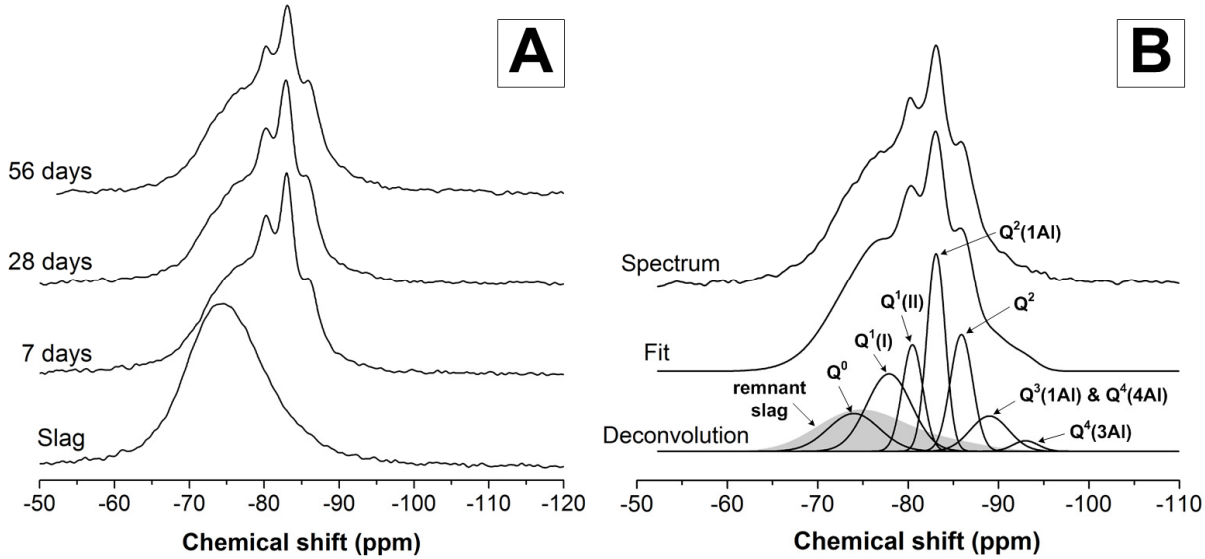

Figure 6. ^{29}Si MAS NMR spectra of sodium silicate-activated slag pastes as a function of the time of curing: (A) as a function of the time of curing; (B) deconvoluted spectrum for the 56 day cured sample.

Table 1. Summary of Q^n environments identified in ^{29}Si MAS NMR spectra of alkali-activated slag pastes as a function of the time of curing. Estimated uncertainty in site percentages is ± 1%, based on the influence of the signal/noise ratio of the spectra on the deconvolution procedures.

age	unreacted slag	reaction products							
		Q^0	Q^1(I)	Q^1(II)	Q^2(1Al)	Q^2	Q^3(1Al)	Q^4(4Al)	Q^4(3Al)
		-74 ppm	-78 ppm	-80 ppm	-83 ppm	-86 ppm	-89 ppm*	-89 ppm*	-93 ppm
unreacted	100	-	-	-	-	-	-	-	-
7 days	39	4	14	11	18	11	4	-	-
28 days	24	7	18	13	22	12	5	-	-
56 days	21	10	18	11	19	13	5	2	1

* A single peak at -89 ppm is used to describe both Q^3(1Al) and Q^4(4Al) components as discussed in the text

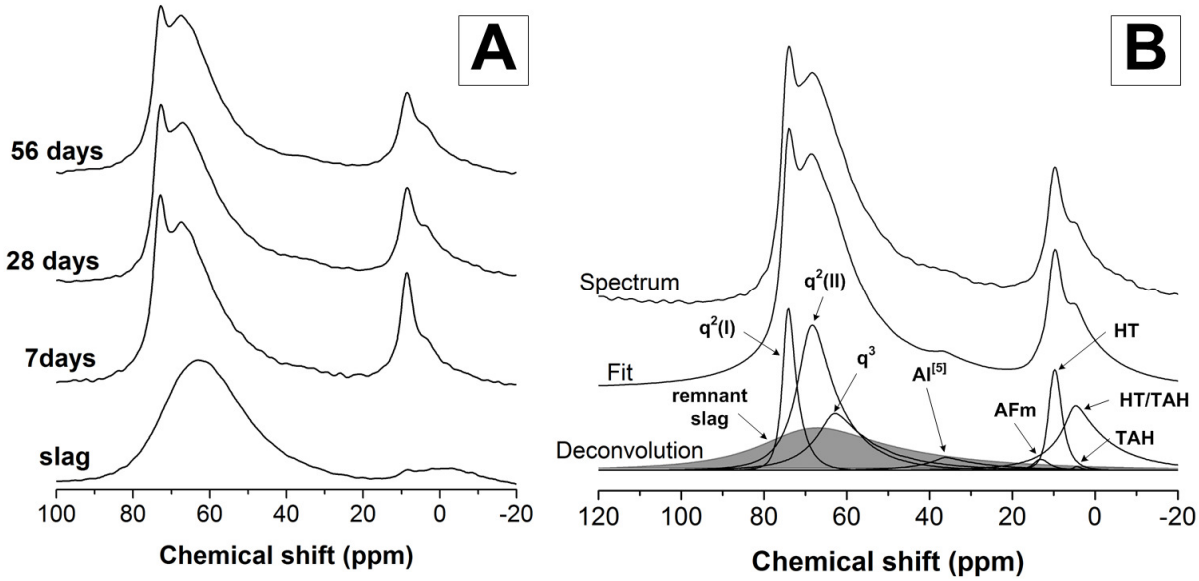

Figure 7. ^{27}Al MAS NMR spectra of the sodium silicate-activated slag pastes: (A) as a function of the time of curing; (B) deconvoluted spectrum for the 56 day cured sample.

Table 2. Summary of Al coordination environments identified in ^{27}Al MAS NMR spectra of the alkali-activated slag pastes as a function of the time of curing. Estimated uncertainty in site percentages is ± 1%, based on the influence of the signal/noise ratio of the spectra on the deconvolution procedures. HT represents hydrotalcite.

age	tetrahedral Al in unreacted slag	q^2(I)	q^2(II)	q^3	$Al^{[5]}$	AFm	HT	HT/ TAH	TAH
	66 ppm	73 ppm	67 ppm	62 ppm	35 ppm	12 ppm	8.7 ppm	3.9 ppm	3.1 ppm
unreacted	100	-	-	-	-	-	-	-	-
7 days	44	10	22	6	0	1	7	10	≤0.1
28 days	26	10	26	14	3	1	6	14	≤0.1
56 days	23	10	28	17	2	1	6	13	≤0.1

The ^{27}Al MAS NMR spectra in Figure 7 corroborate the formation of secondary phases in addition to C-(N)-A-S-H in the AAS, as identified by ESEM-EDS in this study and by X-ray diffraction elsewhere,[16,17,24,42] as there are significant contributions from six-coordinated aluminum ($Al^{[6]}$). The presence of $Al^{[6]}$ in the interlayer and structural incorporation of these species into C-(N)-A-S-H gel has been hypothesized by some authors,[20,43-45] but $Al^{[6]}$ species are not considered in the CSTM. In a recent study,[43] associations in solid-state 2D ^{27}Al{^{1}H} HETCOR NMR spectra were only observed for bands of narrow line width (which were assigned to AFt/AFm type products and TAH) in the $Al^{[6]}$ region of ^{27}Al MAS NMR spectra. From these data, and from the discussion presented by Andersen et

al.,[22] it may be concluded that there is not a significant degree of substitution of six-coordinated Al^{3+} for Ca^{2+} in the interlayer.

The secondary products containing $Al^{[6]}$ are primarily hydrotalcite, and minor amounts of AFm [24,46,47] and TAH phases [22] are observed. The spectral deconvolutions (Appendix C) also show significant contributions from q^3 Al (where the q^n notation for Al sites is equivalent to the Q^n notation for Si sites [48]), suggesting a high degree of crosslinking. Broad contributions from q^2 Al species indicate significant local disorder in these sites, as Al in C-(N)-A-S-H can coordinate with various cationic species in the interlayer region.

The ^{29}Si MAS NMR spectra (Figure 6 and deconvolutions in Appendix C) show small but distinct contributions from Q^3(1Al) sites, in addition to Q^1, Q^2 and Q^2(1Al) silicate species, indicating high levels of aluminum substitution in the C-(N)-A-S-H type gel. The intensity band at -74 ppm is tentatively assigned to Q^0 species, without precluding the possibility of some of the intensity in this peak also representing Q^1(1Al) or Q^1 species (due to the various charge-balancing cations present in the system). This peak has previously been identified in deconvoluted ^{29}Si MAS NMR spectra of sodium silicate-activated GBFS pastes when the anhydrous slag components were scaled to match the reaction extent of the slag calculated from scanning electron microscopy image analysis,[49] but no definitive assignment for this band has been established to date. Although the absolute concentrations of Q^3(1Al) sites are low, the structural constraints of crosslinked C-(N)-A-S-H (Figure 3 and eqs.(22-25)) lead to the calculation of high levels of crosslinking between aluminosilicate chains in C-(N)-A-S-H, as will be discussed in detail below. The ^{29}Si MAS NMR spectra also show non-zero levels of intensity at chemical shifts of approximately -93 ppm, indicating the presence of Q^4(3Al) units in the binder gel. This assignment necessitates contributions from at least one additional four-connected silicate unit (Q^4 type) in the experimental spectra.[50] It was therefore assumed that Q^4(4Al) species were present the ^{29}Si MAS NMR spectra, which is consistent with the significant levels of intensity in the low-ppm range (52-62 ppm) for four-coordinated Al species as observed by ^{27}Al MAS

411 NMR, statistical thermodynamic model predictions [50] and experimental NMR data [51] for Al-rich
412 metakaolin-based geopolymers. Full details regarding this assignment are provided in Appendix C.

413 The Al/Si molar ratios of the C-(N)-A-S-H gel, which can be viewed as the trendline intercepts in
414 Figure 4 for the AAS pastes studied here because the amounts of Mg-free secondary products are
415 minor (≤1% of the total Al intensity for each sample), are in the range $0.19 \leq Al/Si \leq 0.26$; Ca/Si molar
416 ratios vary from approximately $0.8 \leq Ca/Si \leq 1.2$ with the exception of the 7 day sample where Ca/Si
417 ratios up to 1.4 are observed. The trendlines drawn in Figure 4 do not preclude very low levels of
418 Mg-Ca substitution in the C-(N)-A-S-H gel. These measured chemical compositions correlate well
419 with previous studies of AAS where chemical compositions of $0.20 < Al/Si < 0.25$ and $0.8 < Ca/Si < 1.2$
420 are consistently reported for AAS binders produced from GBFS with moderate aluminum (12-14
421 wt.%) and magnesium (7-9 wt.%) content.[13,14,16-19,46]

422 The CSTM, when applied to the ^{29}Si MAS NMR spectral deconvolution data presented in Table 1,
423 yields the results shown in Table 3.

Table 3. The calculated output of the CSTM from the ^{29}Si MAS NMR spectra given in Table 2. A constant interlayer calcium content of $\varphi = \omega = 0.25$ and the maximum partitioning of Q^1 sites into the crosslinked tobermorite phase (i.e. maximizing η) is specified for all pastes.

curing time	species	η	Q^1	$Q^2(1Al)$	Q^2	$Q^3(1Al)$	Q^3	MCL	$\frac{Al}{Si}$	$MCL_{C(N)ASH}$	$\left(\frac{Al}{Si}\right)_{C(N)ASH}$	$\frac{Ca}{Si}$	$\frac{Ca}{Al+Si}$	$\left(\frac{Ca}{Si}\right)_{C(N)ASH}$	$\left(\frac{Ca}{Al+Si}\right)_{C(N)ASH}$
7 days	non-crosslinked	0.60	0.098	0.10	0.033	0	0	5.8	0.22	7.6	0.15	1.1	0.88	1.0	0.86
	crosslinked		0.15	0.074	0.074	0.037	0	10	0.11			0.94	0.85		
28 days	non-crosslinked	0.72	0.085	0.11	0.016	0	0	6.2	0.26	8.3	0.16	1.1	0.87	0.99	0.86
	crosslinked		0.22	0.11	0.11	0.054	0	10	0.11			0.94	0.85		
56 days	non-crosslinked	0.68	0.092	0.086	0.035	0	0	5.6	0.20	7.9	0.14	1.1	0.88	0.98	0.86
	crosslinked		0.20	0.099	0.099	0.049	0	10	0.11			0.94	0.85		

The calculated chemical compositions of the C-(N)-A-S-H phase (Table 3) agree well with the chemistry of laboratory-synthesized C-(N)-A-S-H products, where the molar Al/Si ratio of phase-pure C-(N)-A-S-H has generally been found to be less than or equal to 0.20 for Ca/(Al+Si) molar ratios relevant in AAS systems ($0.7 \leq Ca/(Al+Si) \leq 1.3$).[12,13,20,38] The formation of strätlingite (an AFm phase) is typically observed in activated slag binders if the Al/Si molar ratio is higher than this.[12] This must then be contrasted with the results presented in Table 3, which show that the CSTM can reproduce the experimentally observed Ca/Si ratios, but does not agree with the Al/Si molar ratios for the magnesium-free C-(N)-A-S-H phases and the real AAS binder gels as identified by ESEM-EDS (Figure 4). In all cases the aluminum content of the C-(N)-A-S-H phase is significantly underestimated by the assumption that all of the tetrahedral Al is contained within tobermorite-type phases.

This disagreement is also corroborated by calculation of the average compositions of the binder gels using the experimentally determined extents of reaction of the GBFS precursors in these samples (as determined from the ^{29}Si MAS NMR spectral deconvolutions (Table 1)), which give overall Al/Si molar ratios of 0.396, 0.413 and 0.415 for the binder gels in the 7, 28 and 56 day samples respectively (Figure 5). These ratios are calculated from the elemental compositions of the mix formulations, assuming congruent dissolution of the fraction of the slag which has reacted, and full incorporation of the silica supplied by the activator into the binder, but without distinction between Al in C-(N)-A-S-H or secondary phases.

However, the contributions of secondary phases to the AAS binder are evident in the ^{27}Al MAS NMR spectra (Figure 7), which show that aluminum present in secondary products corresponds to between 18% and 20% of the total Al in these systems. The ^{27}Al MAS NMR spectral deconvolutions also show that hydrotalcite is always the dominant secondary phase in these systems, contributing ≥92% of the $Al^{[6]}$ present in the samples (Table 2). The hydrotalcite product can therefore be expected to account for up to 24-29% of the aluminum in the binder gel (i.e. excluding contributions from remnant GBFS particles). Using this information to correct the Al/Si molar ratios predicted by

453 the CSTM to account for the presence of hydrotalcite gives Al/Si molar ratios of 0.22, 0.22 and 0.18
454 for the sum of the C-(N)-A-S-H and hydrotalcite components of the binder, after 7, 28 and 56 days
455 respectively. Incorporation of AFm, five-coordinated aluminum ($Al^{[5]}$) and TAH phases (assuming that
456 the TAH phase is not silicon-bearing), which are minor (≤4% of total Al intensity for each sample),
457 would give a slight further increase in the calculated Al/Si molar ratios for the AAS binder, but the
458 variable or unknown chemistry of each of these phases prevents their use in direct calculations at
459 this time.

460 In any case, it is unlikely that inclusion of these phases in the calculations would be sufficient to
461 increase the Al/Si molar ratio of the binder, compared to the predictions based on the combination
462 of C-(N)-A-S-H and hydrotalcite phases, to a large enough extent to reconcile the difference between
463 the average composition of the binder as determined by ESEM-EDS and the calculated composition
464 from the CSTM (see Figure 4 and Table 3). It is therefore evident that the bulk composition of the
465 AAS binder, as identified by ESEM-EDS, cannot be adequately explained solely as a C-(N)-A-S-H
466 product.

467 Possible explanations for this discrepancy, given that recent developments in the literature strongly
468 support the presence of crosslinked aluminosilicate chains in the C-(N)-A-S-H product in AAS
469 systems, include:

470 i) significant, non-zero amounts of four-coordinated aluminum ($Al^{[4]}$) species substituting
471 into paired sites in C-(N)-A-S-H;
472 ii) the interlayer region containing significant amounts of aluminum; or
473 iii) the presence of an aluminum-rich gel that is more crosslinked than C-(N)-A-S-H, but is
474 poorly ordered and is present in sufficiently low quantities so as to be not readily
475 identifiable through XRD, ESEM-EDS, ^{27}Al MAS NMR or ^{29}Si MAS NMR experiments.

The possibility that $Al^{[4]}$ species can be substituted into paired sites in C-(N)-A-S-H chains has been previously explored in the literature;[52] inclusion of these species in the CSTM model would lead to an increase in the calculated Al/Si molar ratio for the C-(N)-A-S-H phase because crosslinked structures that include Al substitution in paired sites can accommodate a much higher concentration of Al. However, the presence of $Al^{[4]}$ in paired sites is believed to be strongly disfavored in C-(N)-A-S-H chains.[41] Using atomistic simulations, Manzano et al.[52] concluded that $Al^{[4]}$ substitution in paired sites in C-(N)-A-S-H gel was possible, depending on the Al content of the gel, but only reaching significant concentrations at Al contents notably higher than those which are generally observed in C-(N)-A-S-H gels in experimental studies. Other atomistic simulations of aluminum substitution into silicate chains have identified a thermodynamic preference for the bridging site over the paired site in isolated pentameric chains,[53] and also in pentameric chains confined within an environment representative of 14Å tobermorite,[44] indicating that it is unlikely that Al in paired sites will be a major contributor to the chemistry of AAS gels. Substitution of a small amount of Al into a fraction of the paired sites cannot be entirely discounted, but it is unlikely that these species could solely account for the significant differences between calculated and experimental Al/Si ratios found here.

The possibility that aluminum can act as a charge-balancing species in the interlayer region has been discussed in the literature,[12,20,22] but is not included in the CSTM. Interlayer aluminum has been hypothesized to exist as $Al^{[5]}$,[12,22] because $Al^{[4]}$ is anionic and thus cannot act as a charge-balancer for anionic chain sites, while six-coordinated Al has been proposed to be present in the interlayer,[43,44] but is not considered in the CSTM as discussed above. The potential contributions of these species in the composition of the gel binder can thus be determined from the ^{27}Al MAS NMR spectral deconvolutions, particularly in the $Al^{[5]}$ region of the spectra. However, it is evident that inclusion of interlayer aluminum species will not resolve the significant discrepancies between the modeled and experimentally measured compositions of these AAS binders, as this difference is founded in the $Al^{[4]}$ concentrations alone.

Having eliminated the other possible Al-containing phases from consideration, it is therefore proposed that an additional aluminum-containing activation product must be present as a reaction product in the AAS binder gel. This phase must be long-range disordered, and probably has a characteristic size on the order of nanometers so as to not be observable in ESEM-EDS, TEM-EDS or XRD experimental results. This product is also not readily detectable in ^{27}Al or ^{29}Si MAS NMR spectra, most likely due to its presence at a low concentration with peaks overlapping those assigned to the established silicate and aluminate species in C-(N)-A-S-H type gels. The most likely answer is that some part of the intensity in the ^{29}Si bands at -89 ppm and -93 ppm is actually representing Q^4(4Al) or Q^4(3Al) silicate species in this additional phase, and that a fraction of the ^{27}Al peak assigned to the q^3 aluminate species is also related to this product. An obvious candidate for such an assignment would be a disordered nanoparticulate zeolite-like product with Si/Al ratio close to 1, similar to the conceptual structural model which has been proposed for gels formed through alkali-activation of low-calcium aluminosilicate precursors.[54] Such an assignment would be consistent with the fact that crystalline zeolites are sometimes observed in AAS binders, particularly in systems where there is insufficient Mg to form hydrotalcite.[23,55] This strongly supports the inclusion of Q^4(3Al) and Q^4(4Al) species in the deconvolution results for the 56 days sample (Table 1 and Appendix C).

However, the assignment of some of the Q^3(1Al) (or Q^3) intensity in the ^{29}Si MAS NMR spectra to a phase other than C-(N)-A-S-H would indicate that crosslinking between aluminosilicate chains in the C-(N)-A-S-H product may occur to a lower extent than would be predicted based on complete assignment of Q^3, Q^3(1Al) and q^3 silicate and aluminate species to C-(N)-A-S-H. This is actually to some extent consistent with the observations of low or zero concentrations of Q^3 and Q^3(1Al) silicate species in some hydroxide-activated slag cements,[41] because the chemistry of the binder gels in these systems can be well explained by existing non-crosslinked tobermorite structural models.[32] Contributions assigned to q^3, Q^3 and Q^3(1Al) species are typically observed in ^{27}Al MAS NMR and ^{29}Si MAS NMR spectra of AAS cement pastes activated by alkali silicate solutions,[15,21,56,57] but non-zero intensities for silicate and aluminate species in crosslinked sites have also been observed in

laboratory-synthesized and hydroxide-activated slag pastes.[12,38,56,58] The increased intensity of the bands in the regions traditionally assigned to crosslinked C-(N)-A-S-H species suggest that this additional Al-rich, potentially zeolite-like phase will be more prevalent in silicate-activated AAS systems.

Therefore, the application of the CSTM to the analysis of experimental NMR data does provide a strong indication of the presence of an Al-rich phase distinct from the C-(N)-A-S-H in silicate-activated slag binders, because the structure of tobermorite-like chains is unable to accommodate as much Al as is supplied by the slag precursor in this system. This means that the model predictions of the degree of crosslinking between chains in AAS should be viewed as an upper bound, rather than as an exact value. However, it is clear that a mixture of crosslinked and non-crosslinked tobermorite-like structures provides a more readily generalized view of the chemistry of C-(N)-A-S-H gels than the previous models based solely on the non-crosslinked silicate chain structure. This is likely to be useful in application to blends of Portland cement with siliceous supplementary cementitious materials, in addition to the alkali-activated slag systems discussed here.

5. Conclusions

This paper has presented a generalized model for the chemistry of tobermorite-like calcium (sodium) aluminosilicate hydrate gels, incorporating the possibility of crosslinking between tobermorite chains to better describe the chemistry of high-Al binder systems. The model is named the 'Crosslinked Substituted Tobermorite Model', CSTM. The structures modeled in the CSTM are consistent with Loewenstein's rule of Al-O-Al avoidance, and exclude aluminum substitution into paired tetrahedra. The partitioning of Al into secondary phases such as hydrotalcite is considered through the use of ^{27}Al MAS NMR spectra to identify the concentrations of Al in different coordination states.

The CSTM differs from previous models for the C-(N)-A-S-H phase, which are primarily based on non-crosslinked tobermorite structures, and so is more consistent with recent developments regarding

551 the density and structure of the C-(N)-A-S-H product in alkali-activated slag. The CSTM model
552 represents the first time that a mixture of non-crosslinked and crosslinked C-(N)-A-S-H structures has
553 ever been studied over the full range of compositions observed in AAS systems. The CSTM provides
554 support for aluminosilicate chain crosslinking in the C-(N)-A-S-H phase found in AAS cement, but also
555 provides strong indications of the presence of an additional aluminum-containing activation product
556 in alkali silicate-activated slag binders. This study therefore provides a profoundly deeper and more
557 detailed description of the binder gel chemistry in alkali-activated slag when compared with the
558 existing literature in this area, and is more readily reconciled with the recent developments in the
559 literature.

560 ## 6. Supporting information

561 Additional material is provided in the supporting information document: application of the CSTM to
562 a crosslinked tobermorite species (Figure S1) is presented in Appendix A; derivation of the Ca/Si and
563 Ca/(Al+Si) relationships for a mixture of 9Å, anomalous 11Å, normal 11Å and 14Å tobermorites
564 (eqs.(S1-S13)) is provided in Appendix B; and details related to the experimental procedure and
565 materials (Table S1), the alternative site assignments specified in this study (Table S2 and eq.(S14)),
566 quadrupolar coupling parameters used in this work (Table S3), and spectral deconvolutions of ^{29}Si
567 MAS NMR spectra (Figure S2) and ^{27}Al MAS NMR spectra (Figure S3) are given in Appendix C. A
568 spreadsheet containing the CSTM is also provided to complement the work discussed in this paper.
569 This material is available free of charge via the Internet at http://pubs.acs.org.

570 ## 7. Acknowledgements

571 This work was funded in part by the Australian Research Council (ARC), including support through a
572 Linkage Project co-funded by Zeobond Pty Ltd, and through the Particulate Fluids Processing Centre,
573 a Special Research Centre of the ARC. We thank Dr John Gehman (Bio21 Institute/School of
574 Chemistry, University of Melbourne) for useful discussions and assistance with NMR spectroscopy

and data processing, and Mr Roger Curtain (Bio21 Institute, University of Melbourne) and the Electron Microscopy Unit for assistance in the SEM work. Funding support provided by the University of Sheffield is also gratefully acknowledged.

8. References

(1) Moir, G., Cements. In *Advanced Concrete Technology: Constituent Materials*, Newman, J.; Choo, B. S., Eds. Butterworth-Heinemann: Oxford, 2003; pp 1-45.

(2) Taylor, H. F. W., *Cement Chemistry*. 2nd ed.; Thomas Telford Publishing: London, 1997.

(3) Richardson, I. G., The calcium silicate hydrates. *Cem. Concr. Res.* **2008**, *38*, 137-158.

(4) Juenger, M. C. G.; Winnefeld, F.; Provis, J. L.; Ideker, J. H., Advances in alternative cementitious binders. *Cem. Concr. Res.* **2011**, *41*, 1232-1243.

(5) Lothenbach, B.; Scrivener, K.; Hooton, R. D., Supplementary cementitious materials. *Cem. Concr. Res.* **2011**, *41*, 1244-1256.

(6) Wang, S.-D.; Pu, X.-C.; Scrivener, K. L.; Pratt, P. L., Alkali-activated slag cement and concrete: a review of properties and problems. *Adv. Cem. Res.* **1995**, *7*, 93-102.

(7) Shi, C.; Krivenko, P. V.; Roy, D., *Alkali-Activated Cements and Concretes*. Taylor & Francis: New York, 2006.

(8) Bernal, S. A.; Provis, J. L.; Rose, V.; Mejía de Gutiérrez, R., High-resolution X-ray diffraction and fluorescence microscopy characterization of alkali-activated slag-metakaolin binders. *J. Am. Ceram. Soc.* **2013**, in press, DOI: 10.111/jace.12247.

(9) Skibsted, J.; Andersen, M. D., The Effect of Alkali Ions on the Incorporation of Aluminum in the Calcium Silicate Hydrate (C–S–H) Phase Resulting from Portland Cement Hydration Studied by ^{29}Si MAS NMR. *J. Am. Ceram. Soc.* **2013**, *96*, 651-656.

(10) Chen, W.; Brouwers, H. J. H., The hydration of slag, part 1: Reaction models for alkali-activated slag. *J. Mater. Sci.* **2007**, *42*, 428-443.

(11) Richardson, I. G., Tobermorite/jennite- and tobermorite/calcium hydroxide-based models for the structure of C-S-H: Applicability to hardened pastes of tricalcium silicate, β-dicalcium silicate, Portland cement, and blends of Portland cement with blast-furnace slag, metakaolin, or silica fume. *Cem. Concr. Res.* **2004**, *34*, 1733-1777.

(12) Sun, G. K.; Young, J. F.; Kirkpatrick, R. J., The role of Al in C-S-H: NMR, XRD, and compositional results for precipitated samples. *Cem. Concr. Res.* **2006**, *36*, 18-29.

(13) Pardal, X.; Pochard, I.; Nonat, A., Experimental study of Si-Al substitution in calcium-silicate-hydrate (C-S-H) prepared under equilibrium conditions. *Cem. Concr. Res.* **2009**, *39*, 637-643.

(14) Richardson, I. G.; Brough, A. R.; Groves, G. W.; Dobson, C. M., The characterization of hardened alkali-activated blast-furnace slag pastes and the nature of the calcium silicate hydrate (C-S-H) phase. *Cem. Concr. Res.* **1994**, *24*, 813-829.

(15) Schneider, J.; Cincotto, M. A.; Panepucci, H., ^{29}Si and ^{27}Al high-resolution NMR characterization of calcium silicate hydrate phases in activated blast-furnace slag pastes. *Cem. Concr. Res.* **2001**, *31*, 993-1001.

(16) Ben Haha, M.; Le Saout, G.; Winnefeld, F.; Lothenbach, B., Influence of activator type on hydration kinetics, hydrate assemblage and microstructural development of alkali activated blast-furnace slags. *Cem. Concr. Res.* **2011**, *41*, 301-310.

(17) Ben Haha, M.; Lothenbach, B.; Le Saout, G.; Winnefeld, F., Influence of slag chemistry on the hydration of alkali-activated blast-furnace slag - Part I: Effect of MgO. *Cem. Concr. Res.* **2011**, *41*, 955-963.

(18) Ben Haha, M.; Lothenbach, B.; Le Saout, G.; Winnefeld, F., Influence of slag chemistry on the hydration of alkali-activated blast-furnace slag — Part II: Effect of Al_2O_3. *Cem. Concr. Res.* **2012**, *42*, 74-83.

(19) Brough, A. R.; Atkinson, A., Sodium silicate-based, alkali-activated slag mortars - Part I. Strength, hydration and microstructure. *Cem. Concr. Res.* **2002**, *32*, 865-879.

(20) Faucon, P.; Delagrave, A.; Petit, J. C.; Richet, C.; Marchand, J. M.; Zanni, H., Aluminum incorporation in calcium silicate hydrates (C-S-H) depending on their Ca/Si ratio. *J. Phys. Chem. B* **1999**, *103*, 7796-7802.

(21) Bonk, F.; Schneider, J.; Cincotto, M. A.; Panepucci, H., Characterization by Multinuclear High-Resolution NMR of Hydration Products in Activated Blast-Furnace Slag Pastes. *J. Am. Ceram. Soc.* **2003**, *86*, 1712-1719.

(22) Andersen, M. D.; Jakobsen, H. J.; Skibsted, J., A new aluminium-hydrate species in hydrated Portland cements characterized by ^{27}Al and ^{29}Si MAS NMR spectroscopy. *Cem. Concr. Res.* **2006**, *36*, 3-17.

(23) Bernal, S. A.; Provis, J. L.; Rose, V.; Mejía De Gutierrez, R., Evolution of binder structure in sodium silicate-activated slag-metakaolin blends. *Cem. Concr. Compos.* **2011**, *33*, 46-54.

(24) Bernal, S. A.; Provis, J. L.; Walkley, B.; San Nicolas, R.; Gehman, J. G.; Brice, D. G.; Kilcullen, A.; Duxson, P.; van Deventer, J. S. J., Gel structure in akali-activated binders based on slag and fly ash, and effects of accelerated carbonation. *Cem. Concr. Res.* **2013**, submitted.

638 (25) Bonaccorsi, E.; Merlino, S.; Kampf, A. R., The crystal structure of tobermorite 14Å
639 (plombierite), a C-S-H phase. *J. Am. Ceram. Soc.* **2005**, *88*, 505-512.

640 (26) McConnell, J. D. C., The hydrated calcium silicates riversideite, tobermorite, and plombierite.
641 *Mineral. Mag.* **1954**, *30*, 293-305.

642 (27) Merlino, S.; Bonaccorsi, E.; Armbruster, T., The real structure of tobermorite 11Å: Normal
643 and anomalous forms, OD character and polytypic modifications. *Eur. J. Mineral.* **2001**, *13*, 577-590.

644 (28) Merlino, S.; Bonaccorsi, E.; Armbruster, T., Tobermorites: Their real structure and order-
645 disorder (OD) character. *Am. Mineral.* **1999**, *84*, 1613-1621.

646 (29) Merlino, S.; Bonaccorsi, E.; Armbruster, T., The real structures of clinotobermorite and
647 tobermorite 9Å: OD character, polytypes, and structural relationships. *Eur. J. Mineral.* **2000**, *12*, 411-
648 429.

649 (30) Manzano, H.; Dolado, J. S.; Ayuela, A., Elastic properties of the main species present in
650 Portland cement pastes. *Acta Mater.* **2009**, *57*, 1666-1674.

651 (31) Oh, J. E.; Clark, S. M.; Wenk, H. R.; Monteiro, P. J. M., Experimental determination of bulk
652 modulus of 14Å tobermorite using high pressure synchrotron X-ray diffraction. *Cem. Concr. Res.*
653 **2012**, *42*, 397-403.

654 (32) Richardson, I. G.; Groves, G. W., The incorporation of minor and trace elements into calcium
655 silicate hydrate (CSH) gel in hardened cement pastes. *Cem. Concr. Res.* **1993**, *23*, 131-138.

656 (33) Kulik, D. A., Improving the structural consistency of C-S-H solid solution thermodynamic
657 models. *Cem. Concr. Res.* **2011**, *41*, 477-495.

658 (34) Richardson, I. G., Nature of C-S-H in hardened cements. *Cem. Concr. Res.* **1999**, *29*, 1131-
659 1147.

(35) García Lodeiro, I.; Fernández-Jimenez, A.; Palomo, A.; Macphee, D. E., Effect on fresh C-S-H gels of the simultaneous addition of alkali and aluminium. *Cem. Concr. Res.* **2010**, *40*, 27-32.

(36) Thomas, J. J.; Allen, A. J.; Jennings, H. M., Density and water content of nanoscale solid C-S-H formed in alkali-activated slag (AAS) paste and implications for chemical shrinkage. *Cem. Concr. Res.* **2012**, *42*, 377-383.

(37) Puertas, F.; Palacios, M.; Manzano, H.; Dolado, J. S.; Rico, A.; Rodríguez, J., A model for the C-A-S-H gel formed in alkali-activated slag cements. *J. Eur. Ceram. Soc.* **2011**, *31*, 2043-2056.

(38) Pardal, X.; Brunet, F.; Charpentier, T.; Pochard, I.; Nonat, A., ^{27}Al and ^{29}Si solid-state NMR characterization of calcium-aluminosilicate-hydrate. *Inorg. Chem.* **2012**, *51*, 1827-1836.

(39) Loewenstein, W., The distribution of aluminum in the tetrahedra of silicates and aluminates. *Am. Mineral.* **1954**, *39*, 92-96.

(40) Tossell, J. A., A theoretical study of the molecular basis of the Al avoidance rule and of the spectral characteristics of Al-O-Al linkages. *Am. Mineral.* **1993**, *78*, 911-920.

(41) Richardson, I. G.; Brough, A. R.; Brydson, R.; Groves, G. W.; Dobson, C. M., Location of aluminum in substituted calcium silicate hydrate (C-S-H) gels as determined by ^{29}Si and ^{27}Al NMR and EELS. *J. Am. Ceram. Soc.* **1993**, *76*, 2285-2288.

(42) Bernal, S. A.; Provis, J. L.; Brice, D. G.; Kilcullen, A.; Duxson, P.; van Deventer, J. S. J., Accelerated carbonation testing of alkali-activated binders significantly underestimates service life: the pore solution chemistry. *Cem. Concr. Res.* **2012**, *42*, 1317-1326.

(43) Rawal, A.; Smith, B. J.; Athens, G. L.; Edwards, C. L.; Roberts, L.; Gupta, V.; Chmelka, B. F., Molecular silicate and aluminate species in anhydrous and hydrated cements. *J. Am. Ceram. Soc.* **2010**, *132*, 7321-7337.

682 (44) Abdolhosseini Qomi, M. J.; Ulm, F. J.; Pellenq, R. J. M., Evidence on the dual nature of
683 aluminum in the calcium-silicate-hydrates based on atomistic simulations. *J. Am. Ceram. Soc.* **2012**,
684 *95*, 1128-1137.

685 (45) Stade, H.; Müller, D., On the coordination of Al in ill-crystallized C-S-H phases formed by
686 hydration of tricalcium silicate and by precipitation reactions at ambient temperature. *Cem. Concr.*
687 *Res.* **1987**, *17*, 553-561.

688 (46) Wang, S. D.; Scrivener, K. L., Hydration products of alkali activated slag cement. *Cem. Concr.*
689 *Res.* **1995**, *25*, 561-571.

690 (47) Schilling, P. J.; Roy, A.; Eaton, H. C.; Malone, P. G.; Brabston, W. N., Microstructure, strength,
691 and reaction products of ground granulated blast-furnace slag activated by highly concentrated
692 NaOH solution. *J. Mater. Res.* **1994**, *9*, 188-197.

693 (48) Harris, R. K.; Samadi-Maybodi, A.; Smith, W., The incorporation of aluminum into silicate
694 ions in alkaline aqueous solutions, studied by aluminum-27 n.m.r. *Zeolites* **1997**, *19*, 147-155.

695 (49) Le Saoût, G.; Ben Haha, M.; Winnefeld, F.; Lothenbach, B., Hydration degree of alkali-
696 activated slags: A ^{29}Si NMR study. *J. Am. Ceram. Soc.* **2011**, *94*, 4541-4547.

697 (50) Provis, J. L.; Duxson, P.; Lukey, G. C.; Van Deventer, J. S. J., Statistical thermodynamic model
698 for Si/Al ordering in amorphous aluminosilicates. *Chem. Mater.* **2005**, *17*, 2976-2986.

699 (51) Duxson, P.; Provis, J. L.; Lukey, G. C.; Separovic, F.; van Deventer, J. S. J., ^{29}Si NMR study of
700 structural ordering in aluminosilicate geopolymer gels. *Langmuir* **2005**, *21*, 3028-3036.

701 (52) Manzano, H.; Dolado, J. S.; Griebel, M.; Hamaekers, J., A molecular dynamics study of the
702 aluminosilicate chains structure in Al-rich calcium silicate hydrate (C-S-H) gels. *Phys. Status Solidi A*
703 **2008**, *205*, 1324-1329.

(53) Manzano, H.; Dolado, J. S.; Ayuela, A., Aluminum incorporation to dreierketten silicate chains. *J. Phys. Chem. B* **2009**, *113*, 2832-2839.

(54) Provis, J. L.; Lukey, G. C.; van Deventer, J. S. J., Do geopolymers actually contain nanocrystalline zeolites? - A reexamination of existing results. *Chem. Mater.* **2005**, *17*, 3075-3085.

(55) Talling, B.; Krivenko, P. V., Blast furnace slag - The ultimate binder. In *Waste Materials Used in Concrete Manufacturing*, Chandra, S., Ed. Noyes Publications: Park Ridge, NJ, 1997; pp 235-289.

(56) Palacios, M.; Puertas, F., Effect of carbonation on alkali-activated slag paste. *J. Am. Ceram. Soc.* **2006**, *89*, 3211-3221.

(57) Fernández-Jiménez, A.; Puertas, F.; Sobrados, I.; Sanz, J., Structure of calcium silicate hydrates formed in alkaline-activated slag: Influence of the type of alkaline activator. *J. Am. Ceram. Soc.* **2003**, *86*, 1389-1394.

(58) Renaudin, G.; Russias, J.; Leroux, F.; Cau-dit-Coumes, C.; Frizon, F., Structural characterization of C-S-H and C-A-S-H samples - Part II: Local environment investigated by spectroscopic analyses. *J. Solid State Chem.* **2009**, *182*, 3320-3329.

720 ***TOC Graphic***

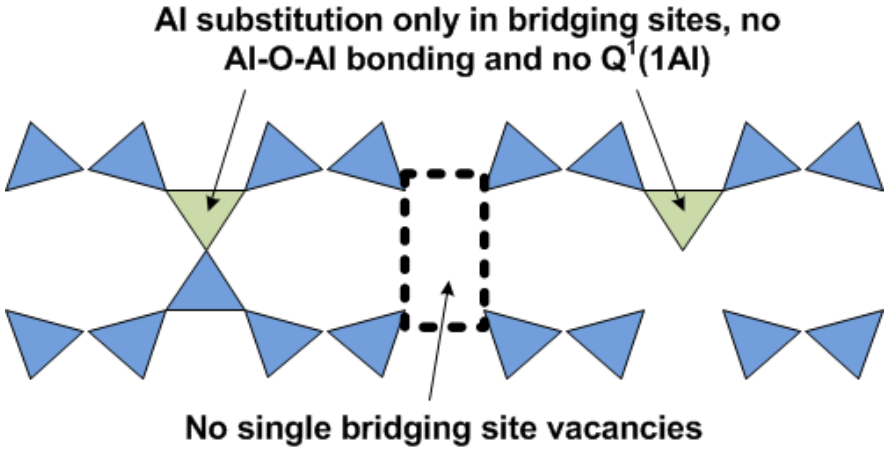

721